

Interfacial reactions between eutectic Sn–Pb solder and Co substrate

Chao-hong Wang · Chun-yi Kuo

Received: 10 August 2010/Accepted: 27 November 2010/Published online: 8 December 2010
© Springer Science+Business Media, LLC 2010

Abstract This study examined the reaction couples of Co substrate with liquid and solid Sn-37 wt% Pb alloys, respectively. In the liquid/solid Sn–Pb/Co couples, one single-phase CoSn_3 layer was found at the interface at temperatures from 210 to 250 °C. The layer thickness was measured as a function of the reaction time. The layer growth rate increased with increasing temperature. The CoSn_3 layer growth was linear in the early stage and then became parabolic. In addition, the similar CoSn_3 growth behavior results were observed in the solid/solid Sn–Pb/Co couples from 150 to 170 °C. Nevertheless, one Pb-rich phase layer accumulated at the solder/ CoSn_3 interface due to Sn consumption. Also, the reaction kinetics of Sn-37 wt% Pb/Co was symmetrically studied at various temperatures. The chemical reaction constants, diffusion constants, and the relevant activation energies were reported.

Introduction

Soldering technology is extensively applied for joining components in the electronics industry [1, 2]. One solder alloy wets a metal substrate to yield a solder joint at an operation temperature above the melting point of solder. Usually, one or more intermetallic (IMC) phases form at the interface between solder and substrate due to atomic diffusion during the soldering process [3]. Conventional eutectic SnPb solder (Sn-37 wt% Pb) has been used for a long time [1]. Nevertheless, many countries have legislation that bans the use of Pb-containing solders due to

environmental concerns [3]. Therefore, various Pb-free solders have been developed to replace the conventional Sn–Pb solder [4, 5].

On the other hand, Cu is widely used as a substrate material and Ni is a common diffusion barrier material. Many studies have investigated the solder joints of the eutectic Sn–Pb solder on Cu or Ni [6–12]. Previous studies have reported that Pb does not actively participate in the IMC formation in the eutectic Sn–Pb/Cu reaction, and only Sn reacts with Cu to produce the Cu_3Sn and Cu_6Sn_5 phase [6, 7]. Similarly, only the formation of the Ni_3Sn_4 phase occurs in eutectic Sn–Pb/Ni [9].

Recently, Co and its alloys, such as Ni–Co alloy, were evaluated for their potential use as diffusion barriers and as under bump metallurgy (UBM) materials [13–17]. In addition, Co and its alloys are often used in surface finish by electroplating due to their superior corrosion resistance [18, 19]. Thus, contact takes place between Co and various solders. The interfacial reaction of Co with solders has been discussed in several studies [20–25], but the research related to this topic is still limited. In our preliminary study, CoSn_3 was the primary reaction phase in the binary solid/solid Sn/Co interfacial reaction [20]. The CoSn_3 IMC growth showed very fast and linear reaction times in the initial stage, and then become parabolic. Particularly, CoSn_3 also exhibits a unique cruciform formation [21]. Nevertheless, minor Cu alloying in Pb-free solders significantly suppresses CoSn_3 growth [22].

Though Sn-37 wt% Pb alloy is no longer used as the principal solder, it is still believed to be important for industrial application. Therefore, a detailed understanding of the interfacial reaction between Co and eutectic Sn–Pb solder is needed to evaluate IMC formation and growth. Up to now, there is, however, no available research on the interfacial reaction of eutectic Sn–Pb solder with Co

C. Wang (✉) · C. Kuo
Department of Chemical Engineering, National Chung Cheng University, Chia-Yi 62102, Taiwan
e-mail: chmchw@ccu.edu.tw

substrate. The objective of this study is to experimentally examine the interfacial reactions of eutectic Sn–Pb solder with Co in two different solid/solid and liquid/solid couples at different temperatures. This study also focuses on examining the kinetics of the IMC formation.

Experimental procedures

Binary Sn-37 wt% Pb alloy was prepared from the respective pure elemental materials (Sn shots: 99.98 wt% purity, Pb shots: 99.95 wt% purity). Appropriate amounts of Sn and Pb were weighed and encapsulated in a quartz tube under a vacuum of 10^{-2} torr. The Sn–Pb alloy was melt and homogenized in a box furnace at 500 °C for 1 week. This sample capsule was then removed from the furnace and quenched in water. The Sn–Pb ingot was cut to several 2 g pieces. In addition, one 0.5 mm-thick Co foil was cut into a dimension of 5 × 20 mm and then it was polished and cleaned. The rosin mildly activated flux (RMA-type) was applied onto the Co substrate. The 2 g Sn–Pb alloy was placed in a quartz tube with 6 mm inside diameter and it was remelted at 250 °C. The Co substrate rinsed with flux was dipped into the molten Sn–Pb alloy and subsequently quenched immediately to finish the preparation of Sn–Pb/Co reaction couple.

The reaction couples were reacted at the two different temperature ranges, 150–170 °C for solid solder/Co reaction and 210–250 °C for liquid solder/Co. In the cases of the solid/solid reactions, the Sn–Pb/Co couples were directly placed in the furnace. In the liquid/solid reactions, the prepared reaction couples must be encapsulated in the quartz tube again to avoid oxidization during the reaction period. After a predetermined reaction time, the reaction couple was removed from the furnace for metallographic observation. The reaction couple was mounted with epoxy resin, cross-sectioned, and polished. The interfacial microstructure of the reaction couple was examined using optical microscopy and scanning electron microscopy (SEM). The electron probe microanalysis (EPMA) was used to precisely analyze the composition of the reaction phase. The image analysis software was employed to measure the average reaction layer thickness. Each thickness value is an average of at least ten measurements at different locations.

Results and discussion

Solid/solid Sn–Pb/Co interfacial reactions

Figure 1a shows the cross-sectional back-scattered electron image (BEI) micrograph of the as-cast Sn-37 wt% Pb/Co

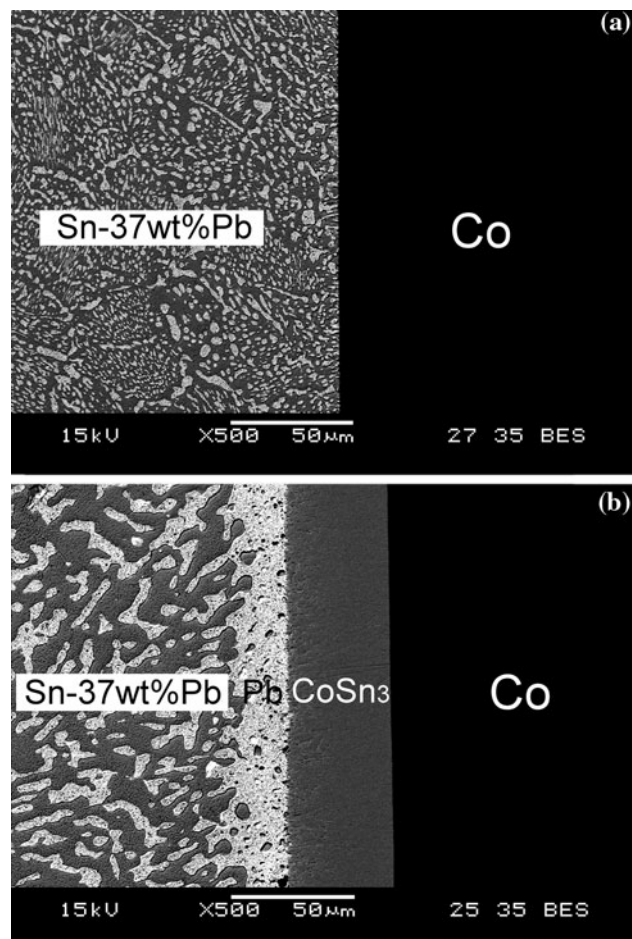


Fig. 1 BEI micrograph of the Sn-37 wt% Pb/Co couple of **a** as-prepared sample and **b** after reaction at 170 °C for 120 h

couple. On the right-hand side, the black phase is the Co substrate. The opposite region exhibits the typical eutectic structure of the Sn-37 wt% Pb alloy. The brighter phase is the Pb-rich phase and the darker matrix phase is the Sn-rich one. No IMC layer was found at the initial interface. After aging at 170 °C for 120 h, the interfacial microstructure of the eutectic Sn–Pb/Co couple is shown in Fig. 1b. One uniform and continuous IMC layer was formed on the Co substrate and its average thickness is about 41 μm. The results of EPMA analysis reveal that the IMC composition is Sn-25.1 at% Co-0.1 at% Pb. The related phase diagram can provide information for determining the IMC phase. Nevertheless, no ternary Sn–Pb–Co phase diagram is presently available. Since the IMC layer has very little Pb solubility, it can refer to the binary Sn–Co phase diagram [26]. Therefore, it can be determined to be a stoichiometric CoSn₃ compound. The CoSn₃ formation in the Sn-37 wt% Pb/Co is the same as that in the Sn/Co reaction [20].

Similar to the Cu and Ni substrates [6–9], the formed IMC species is not affected by Pb, even with such large Pb content. This suggests that Pb has no strong interaction

with Co. In other words, Pb is not involved in the chemical transformation of CoSn_3 . Furthermore, according to the Co–Pb phase diagram [27], there is only one monotectic reaction and there is no intermediate phase. Also, Co and Pb have very little solubility with each other. This implies that the interatomic bond between Co and Pb is repulsive, and thus, Pb is chemically inert to Co. This suggestion is in good agreement with the present interfacial observation.

Remarkably, only one very bright layer exists adjacent to the CoSn_3 layer, as seen in Fig. 1b. It is determined to be Pb-rich phase with close to saturated Sn solubility of about 25 at%. Moreover, some small Sn-rich phase particulates are dispersed in the Pb-rich layer. The CoSn_3 layer has very limited Pb content. This means that both Sn and Co are major reacting elements. In addition, Sn is the dominant diffusion element since the CoSn_3 growth front was found occurring at the CoSn_3/Co interface. As the CoSn_3 phase grows, only the Sn of the solder is consumed. As a result, the remnant unreacted Pb phase accumulated and gradually thickened with reaction time owing to the great expense of Sn. This reaction process must obey the mass balance law. Every 10 μm thick formation of the CoSn_3 layer needs to consume a 9.7 μm thick Sn layer. Therefore, for the eutectic Sn–Pb solder, the accumulated Pb layer is calculated to be about 3.6 μm thick. Consequently, it is quite reasonable that the thickness ratio of Pb to CoSn_3 observed in Fig. 1b is consistent with the theoretical value.

To observe whether the IMC formation exhibited a cruciform pattern, the rectangular Co substrate was carefully prepared with right angles and a polished surface. The reaction was conducted at 170 °C for 792 h. As shown in Fig. 2a, clearly, no reaction product formed at the corners, which is the feature of cruciform pattern formation. Unlike the cruciform pattern observed in the Sn/Co couple at 200 °C, the endpoints of the IMC layers at the corners, representing the beginning for layer growth, are still joined together. This observation implies that the pile-up stress within the reaction layer was not large enough to cause solder alloy deformation at the corners, so the endpoints had not yet completely split.

Figure 2b and c is the local magnified micrographs of the reaction layers at the left interface and the upper one, respectively. Notably, the reaction layers were filled up with bright Pb-rich phase, which were marked within a dashed line rectangle, but the microstructures were different. As shown in Fig. 2c, the Pb phases appear along the CoSn_3 grain boundaries, perpendicular to the interface. In contrast, the Pb-rich phases are with zigzag pattern and parallel to the interface in Fig. 2b, indicating the CoSn_3 microstructure. The microstructural difference thus provides evidence that the reaction layers were subjected to different interior stresses. This reveals that the reaction layer at the corners (or at the short side) is under tensile stress and thus it leads to CoSn_3 expansion. Eventually, the

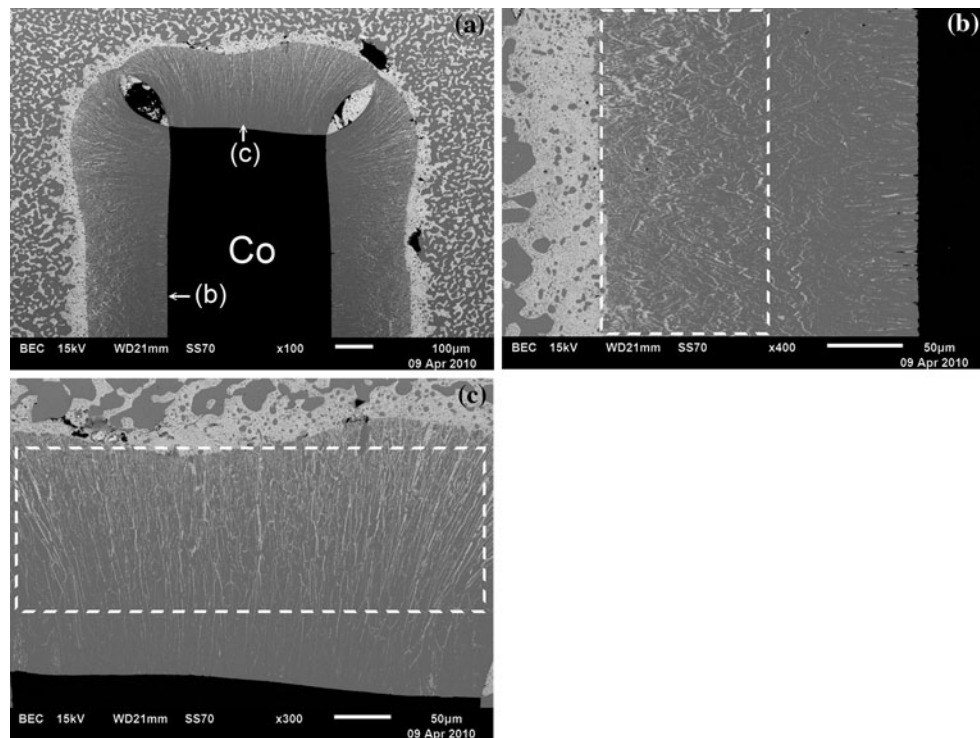


Fig. 2 **a** BEI micrograph of the Sn-37 wt% Pb/Co couple at 170 °C for 792 h, **b** local magnified image of the left interface, and **c** local magnified image of the upper interface

solder atoms, especially Pb, can easily migrate into the grain boundaries. This might relieve the tensile stress. Accordingly, this can also explain why the pile-up stress is not sufficient to separate the endpoint between the layers. Moreover, it is worth noting that the reaction layer at the corners is much thicker than that at the lateral interface. The faster IMC growth could be because the Pb-rich phases at the grain boundaries provide more diffusion paths for Sn.

To further investigate the IMC growth kinetics, it is necessary to measure the IMC layer thickness at different durations of reaction time. In previous studies, the results for different reaction times have conventionally been obtained from different couples. Nevertheless, this often causes larger variations. To eliminate the discrepancy between different couples, this study applies the method of consecutive measurements on the same reaction couples. This helps to precisely observe the thickness changes that occur during the IMC growth period. Heat treatments in the furnace and thickness measurements were carried out repeatedly on the same couple. In addition, at least three different couples were conducted to check the validity and consistency of measured data. The reactions were performed at various temperatures, 150, 160, and 170 °C, respectively. Similarly, only the CoSn₃ layer was formed. The plot of the IMC thickness against the reaction time is shown in Fig. 3a–c. The reaction layer grows thicker with increasing reaction time as well with higher reaction temperatures. For example, at the same reaction time of 72 h,

the layer thicknesses are 7.3, 14.2, and 32.1 μm at 150, 160, and 170 °C, respectively.

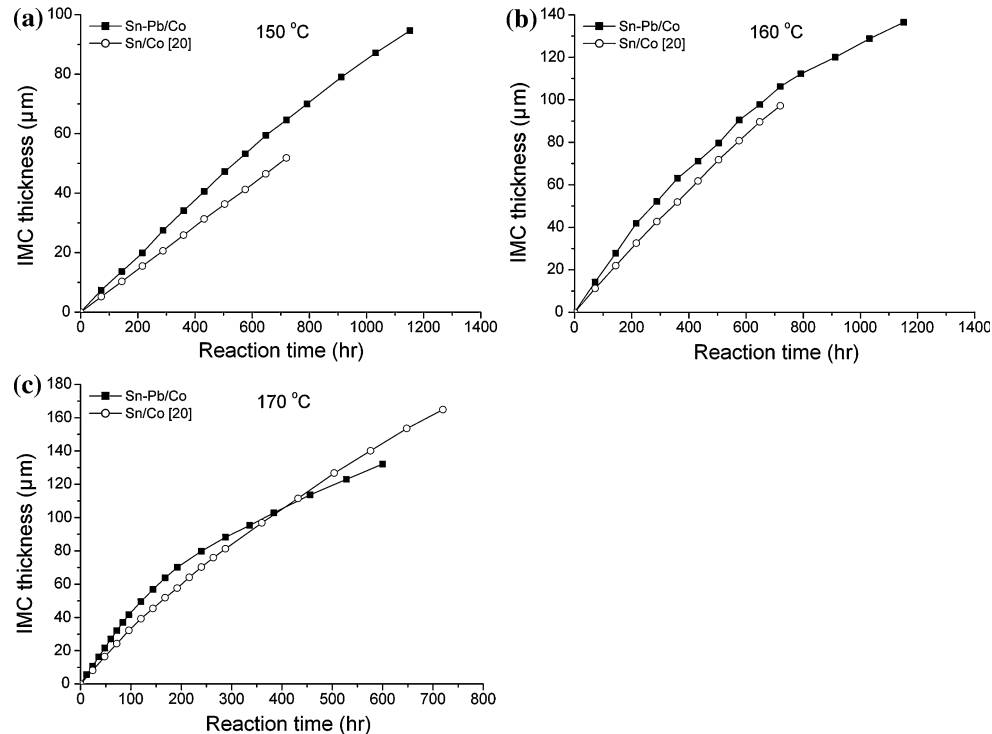
For comparison, the growth data for the Sn/Co interfacial reactions [20] are also shown in Fig. 3. The growth rate of the Sn–Pb/Co couples is slightly higher than that of the Sn/Co couples. In the reaction at 170 °C, the reaction layer in the Sn–Pb/Co is thinner than that of Sn/Co after 360 h of reaction. Furthermore, the reaction layer growth of Sn–Pb/Co at 170 °C appears linear with the reaction time in the initial 72 h of reaction. After that, it gradually becomes parabolic. This similar growth behavior was also found in the prior Sn/Co interfacial system [20]. This indicates that CoSn₃ layer growth is reaction controlled and subsequently becomes diffusion controlled. The linear relationship of time–thickness dependence is more significant in the reaction at 150 °C due to slower growth, as displayed in Fig. 3a.

According to Dybkov's reaction diffusion model [28], the IMC layer formation is considered to be governed by two steps, chemical transformation and atomic diffusion. The relationship between the thickness and reaction time can be described by the following equation:

$$t = x/k_{\text{chem}} + x^2/2k_{\text{dif}}, \quad (1)$$

where x is the reaction layer thickness and t is the total reaction time. The k_{chem} is the chemical reaction constant (m s^{-1}), and k_{dif} is the diffusion constant ($\text{m}^2 \text{s}^{-1}$). In the initial stage, the layer growth is linear because it is only

Fig. 3 The plot of the reaction layer thickness against reaction time in the Sn-37 wt% Pb/Co couples reacted at **a** 150 °C, **b** 160 °C, and **c** 170 °C



determined by the chemical transformation at the interface. In the meantime, the layer is so thin that the atomic diffusion is not a dominant step. The layer grows thicker with reaction. Once the thickness exceeds one critical value, the atomic diffusion becomes the rate-determining step.

The initial linear growth of the Sn–Pb/Co couples is clearly exhibited in Fig. 3. Moreover, as shown in Fig. 4a–c, the plot of the square of the reaction layer thickness versus the reaction time reveals the later parabolic growth. According to the above-mentioned IMC growth equation, the chemical reaction constant, k_{chem} , can be determined by slope-fitting on the initial linear portion in Fig. 3a–c. Similarly, the diffusion constant, k_{dif} , can also be obtained from the results in Fig. 4a–c. The respective chemical reaction constants and diffusion constants for various temperatures are summarized in Table 1.

These two constants can be given by an Arrhenius expression:

$$k = k_0 \exp(-Q/RT), \quad (2)$$

where k_0 is the temperature-independent prefactor, Q is the activation energy, R is universal gas constant, and T is the absolute temperature. Figure 5a and b is the plots of the logarithm of the coefficient versus the reciprocal of the absolute temperature for the chemical reaction constant and diffusion constant, respectively. Hence, the slope and the

Table 1 The chemical reaction constants, diffusion constants, and critical thickness in the Sn-37 wt% Pb/Co interfacial reactions at various reaction temperatures

T (°C)	k_{chem} (m s ⁻¹)	k_{dif} (m ² s ⁻¹)	Critical thickness (μm)
150	2.58×10^{-11}	1.51×10^{-15}	58.4
160	5.36×10^{-11}	2.62×10^{-15}	48.8
170	1.21×10^{-10}	4.29×10^{-15}	35.4
210	1.93×10^{-9}	2.98×10^{-13}	154.1
230	6.58×10^{-9}	7.04×10^{-13}	106.9
250	1.50×10^{-8}	1.29×10^{-12}	85.8

intercept can determine the activation energy and the corresponding prefactor, respectively, by fitting a straight line. Accordingly, the activation energy and the prefactor for the chemical reaction constant are 120.4 kJ/mol (1.248 eV) and 18306 m s⁻¹. For the diffusion constant, they are 81.5 kJ/mol (0.845 eV) and 1.76×10^{-5} m² s⁻¹. The relevant values are also summarized in Table 2. The activation energy for the chemical reaction constant is greater than that of the diffusion constant.

As the reaction layer grows above the critical thickness, the chemical transformation-limited interfacial reaction starts to become diffusion-controlled. The critical thickness is defined as $k_{\text{dif}}/k_{\text{chem}}$. Accordingly, the critical thickness

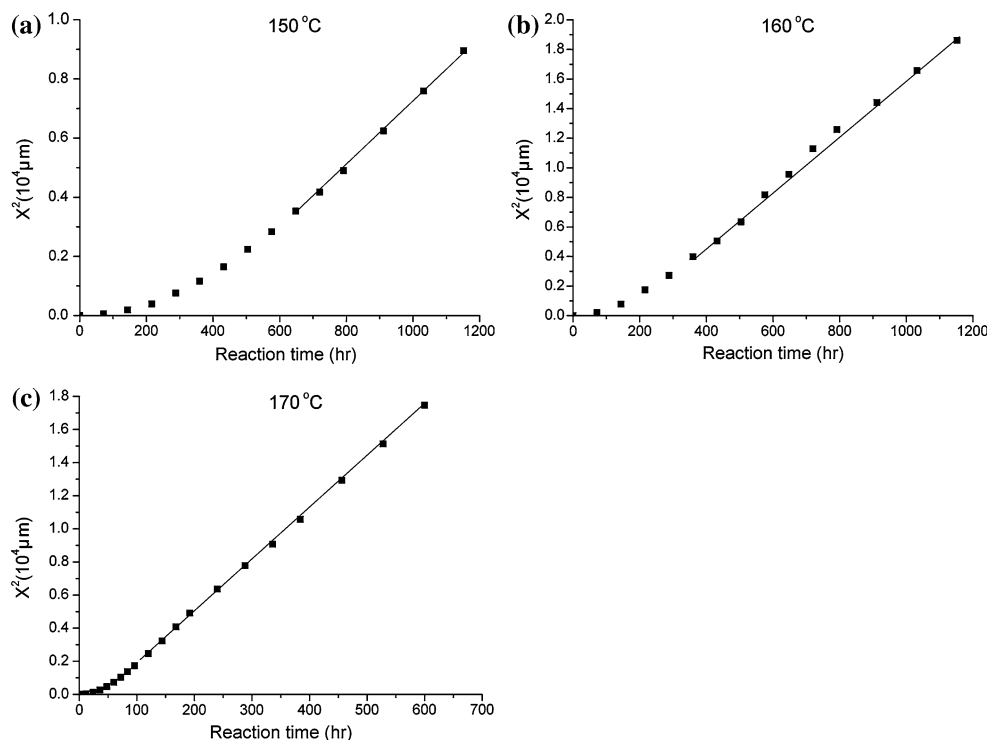


Fig. 4 The plot of the square of the reaction layer thickness versus reaction time in the Sn-37 wt% Pb/Co couples reacted at **a** 150 °C, **b** 160 °C, and **c** 170 °C

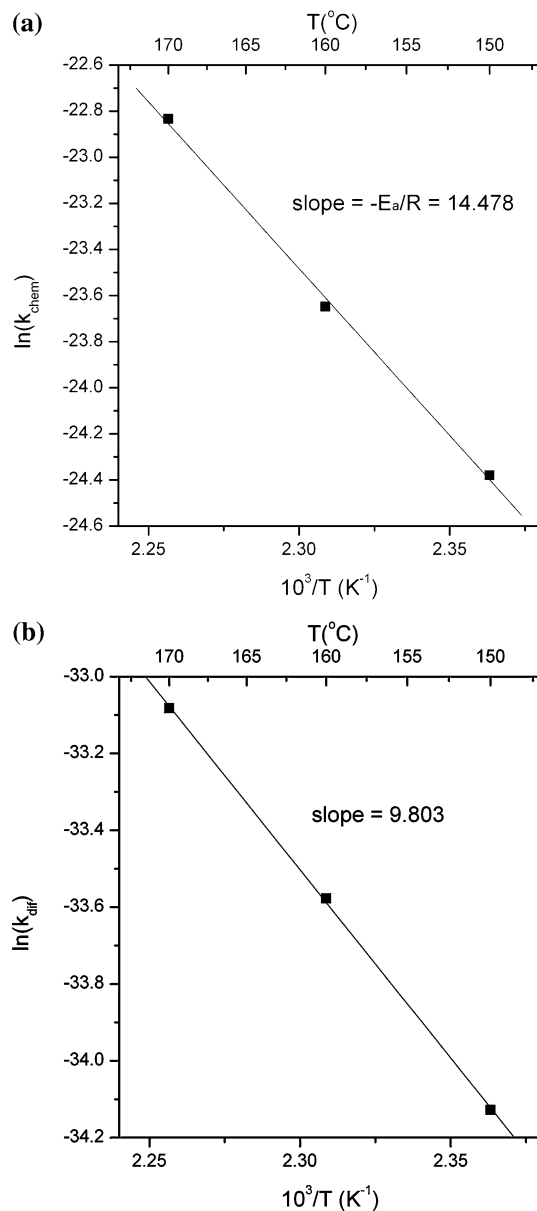


Fig. 5 Arrhenius plot showing temperature dependence of **a** chemical reaction constant and **b** diffusion constant in the solid/solid Sn-37 wt% Pb/Co reaction

can be obtained, as shown in Table 1. It is about 35, 49, and 58 μm for the Sn–Pb/Co reactions at 170, 160, and 150 $^\circ\text{C}$, respectively. The critical thickness increases with decreasing reaction temperature. Nevertheless, a previous study [20] revealed that the critical thicknesses at different reaction temperatures in the Sn/Co couple are almost the same, about 80 μm . The insignificant temperature dependence of the critical thickness occurs because the activation energies of both the chemical reaction and diffusion constant are nearly similar. Accordingly, the critical thickness in the Sn–Pb/Co changes with varying reaction temperatures, which is consistent with the above results suggesting

Table 2 The prefactor and activation energy for the chemical reaction constant and diffusion constant in the Sn-37 wt% Pb/Co interfacial reactions

	Prefactor	Activation energy
Solid/solid reactions		
Reaction constant (k_{chem})	18306 m s^{-1}	120.4 kJ/mol (1.248 eV)
Diffusion constant (k_{dif})	$1.76 \times 10^{-5} \text{ m}^2 \text{ s}^{-1}$	81.5 kJ/mol (0.845 eV)
Liquid/solid reactions		
Reaction constant (k_{chem})	15.33 m s^{-1}	107.8 kJ/mol (1.117 eV)
Diffusion constant (k_{dif})	$6.37 \times 10^{-5} \text{ m}^2 \text{ s}^{-1}$	76.9 kJ/mol (0.797 eV)

that the activation energies for these two constants are significantly different.

Liquid/solid Sn–Pb/Co interfacial reactions

The liquid/solid Sn–Pb/Co interfacial reactions were also conducted above the melting point of eutectic Sn–Pb solders. Figure 6 shows the interfacial microstructure of Sn–Pb/Co after reaction at 250 $^\circ\text{C}$ for 2 h. Similar to the solid/solid interfacial reaction, one uniform CoSn_3 phase layer is found, but the growth rate is much faster. The average thickness is about 110 μm . Nevertheless, unlike the observation in Fig. 1b, the accumulated Pb layer does not appear due to liquid solder reaction. The reactions were carried out with different reaction lengths to investigate the growth rate. Figure 7 shows the average layer thickness versus reaction time at 210, 230, and 250 $^\circ\text{C}$, respectively. In contrast from the measurements of solid/solid reactions, each data point is measured from the different reaction couples. Similar growth behavior is observed. Also, the

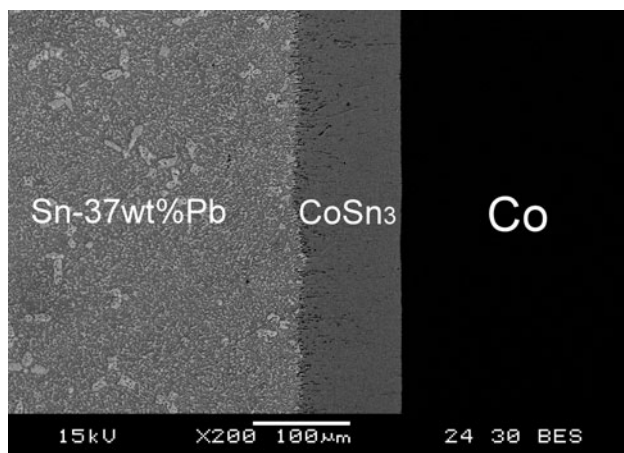


Fig. 6 BEI micrograph of the liquid/solid Sn-37 wt% Pb/Co couple after reaction at 250 $^\circ\text{C}$ for 2 h

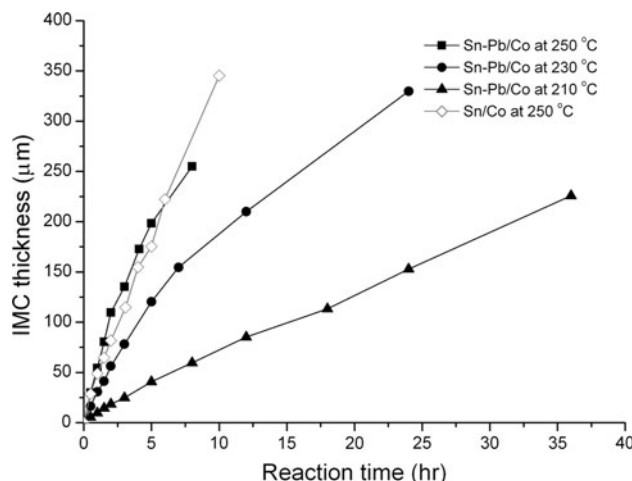


Fig. 7 The plot of the reaction layer thickness against reaction time in the Sn-37 wt% Pb/Co couples at 210, 230, and 250 °C

reaction layer exhibits initial rapid linear growth followed by a parabolic growth. Similar analysis was carried out based on the experimental results. The correlated chemical reaction constants and diffusions at different temperatures are shown in Table 1. For the sake of comparison, the Sn/Co reactions were also preformed at 250 °C. The IMC growth rate is similar to that of Sn–Pb/Co.

The calculated critical thicknesses are about 154, 107, and 86 μm at 210, 230, and 250 °C, respectively, for the liquid/solid Sn–Pb/Co reactions. The critical thickness decreased with higher reaction temperatures. A similar trend was also found in the solid/solid couples. The critical thickness in the liquid/solid Sn–Pb/Co reaction is greater than for the solid/solid reaction. It is likely that the atomic diffusion is relatively much faster in the liquid/solid couple, so the chemical transformation stage becomes more dominant. Accordingly, the critical thicknesses of the liquid/solid reactions are greater. The temperature dependence of the related constants is discussed. Figure 8a and b is the Arrhenius plots for the chemical reaction constant and diffusion constant, respectively. As shown in Table 2, the activation energy for the reaction constant and diffusion constant can be calculated as 107.8 kJ/mol (1.117 eV) and 76.9 kJ/mol (0.797 eV), respectively, and the corresponding prefactors are 15.33 m s⁻¹ and 6.37 × 10⁻⁵ m² s⁻¹, respectively. The activation energy of the reaction constant is higher than that of the diffusion constant. This indicates that the effect of temperature on the chemical reaction constant is greater than on the diffusion constant. Therefore, with increasing reaction temperature, the increment of the reaction constant is larger than that of the diffusion constant, making the diffusion stage become more dominant. Consequently, the critical thickness is reduced at higher temperatures.

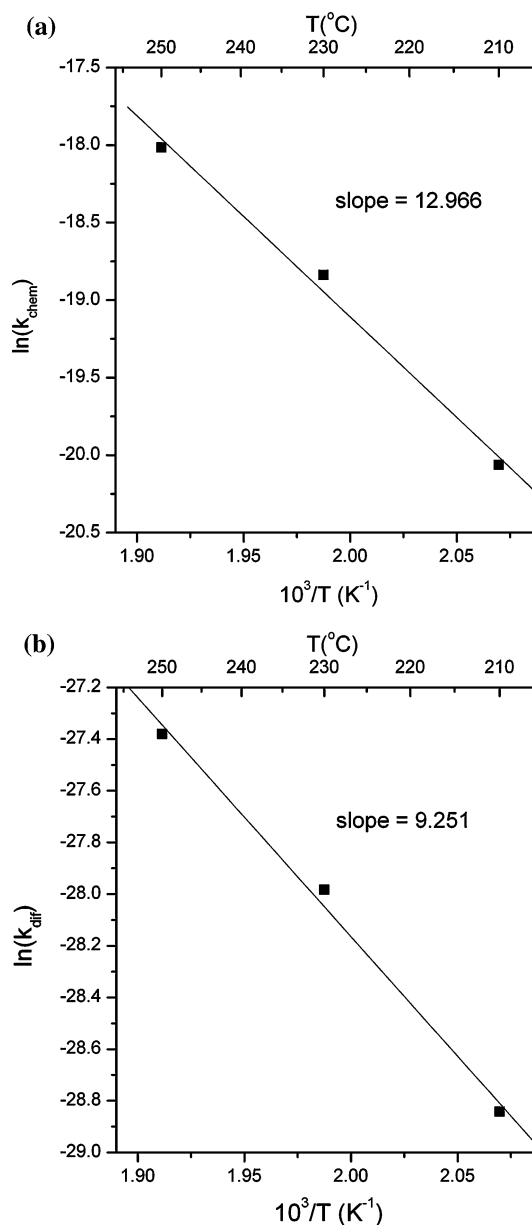


Fig. 8 Arrhenius plot showing temperature dependence of **a** chemical reaction constant and **b** diffusion constant in the liquid/solid Sn-37 wt% Pb/Co reaction

Conclusions

The interfacial reactions of the eutectic Sn–Pb solder and Co substrate have been examined at various temperatures. The intermetallic growth kinetics were analyzed under the two temperature zones, 210–250 °C for molten solder reaction and 150–170 °C for solid-state reaction, respectively. Only one uniform CoSn₃ phase layer was formed. Initially, the CoSn₃ growth is linear with the reaction time. Later, it becomes parabolic. This indicates that the rate-controlling step changes from chemical transformation to atomic diffusion. In addition, the experimental

results regarding temperature dependence reveal that the activation energies for the chemical reaction constant and diffusion constant are 107.8 and 76.9 kJ/mol, respectively, for the liquid/solid reaction, and 120.4 and 81.5 kJ/mol, respectively, for the solid/solid reaction.

Acknowledgements This research funding was supported by the National Science Council of Taiwan (NSC 98-2221-E-194-065).

References

1. Tu KN, Zeng K (2001) Mater Sci Eng R 34:1
2. Ho CE, Yang SC, Kao CR (2007) J Mater Sci Mater Electron 18:155
3. Wang CH, Chen SW (2006) Acta Mater 54:247
4. Chen SW, Wang CH, Lin SK, Chiu CN (2007) J Mater Sci Mater Electron 18:19
5. Islam MN, Chan YC, Rizvi MJ, Jillek W (2005) J Alloys Compd 400:136
6. Tu KN, Gusak AM, Li M (2003) J Appl Phys 93:1335
7. Lee JH, Kim YS (2002) J Electron Mater 31:576
8. Jang GY, Duh JG (2005) J Electron Mater 34:68
9. Chen HY, Chen C (2009) J Electron Mater 38:338
10. Hwang CW, Suganuma K (2004) Mater Sci Eng A 373:187
11. Kim BJ, Lim GT, Kim J, Lee K, Park YB, Lee HY, Joo YC (2009) Met Mater Int 15:815
12. Huang YC, Chen SW, Chang CH, Wu JC, Gierlotka W (2007) J Mater Res 22:2924
13. Labie R, Ratchev P, Beyne E (2005) In: Proceedings in EPTC conference, pp 449–451
14. Chen CC, Chan YT (2010) Intermetallics 18:649
15. Magagnin L, Sirtori V, Seregni S, Origo A, Cavallotti PL (2005) Electrochim Acta 50:4621
16. Liang MW, Yen HT, Hsieh TE (2006) J Electron Mater 35:1593
17. Chao YH, Chen SW, Chang CH, Chen CC (2008) Metall Mater Trans A 39:477
18. Kim SH, Aust KT, Erb U, Gonzales F, Palumbo G (2003) Scripta Mater 48:1379
19. Hamid ZA (2003) Mater Lett 57:2558
20. Wang CH, Chen SW (2008) Intermetallics 16:524
21. Wang CH, Chen SW (2007) J Mater Res 22:3404
22. Wang CH, Kuo CY (2010) J Electron Mater 39:1303
23. Dybkov V (2009) JOM 61:76
24. Zhu W, Liu H, Wang J, Jin Z (2008) J Alloys Compd 456:113
25. Zhu W, Wang J, Liu H, Jin Z, Gong W (2007) Mater Sci Eng A 456:109
26. Vassilev GP, Lilova KI, Gachon JC (2007) Intermetallics 15:1156
27. Massalski TB (1990) Binary alloy phase diagrams, 2nd edn. ASM International, Materials Park, pp 1220–1221
28. Dybkov VI (2002) Reaction diffusion and solid state chemical kinetics. The IPMS Publications, Kyiv, pp 5–20